Programmable Control of Multiscale Droplets using V-Valves

Tian Xue, Ankit Jain, Xiaobao Cao, David Hess, Stavros Stavrakis,* and Andrew de Mello*

Contemporary droplet-based microfluidic platforms generate large numbers of sub-nanoliter ($<10^{-9}$ L) volume droplets on short timescales. The controllable generation of femtoliter (10^{-15} L) volume droplets is however a far more challenging task. Herein, the design, fabrication, and testing of a valve-based droplet-on-demand generator that enables the robust and controllable production of femtoliter-volume water-in-oil droplets is described, where droplet size is determined by on-chip pressure. This generator enables the sequential supply of femtoliter droplets to much larger "mother" droplets stored on-chip, which in turn allows for high-precision droplet dilution and programmable droplet pairing/merging operations. Such an approach can generate in excess of 700 fL-volume droplets of variable content and with dilution factors of almost three orders of magnitude. Using the same principle, the microfluidic platform can also perform rapid, low-volume consumption titrations. Accordingly, the valve-based droplet-on-demand generator allows for a range of automated and multi-step droplet-based manipulations.

1. Introduction

Over the last two decades, microfluidic technologies have emerged as powerful tools for performing high throughput and low-cost bio/chemical reactions. In this regard, droplet-based microfluidic systems have proved especially useful, since large numbers of isolated assay compartments can be generated, loaded, and processed on short timescales.[1–3] Unsurprisingly, droplet-based microfluidic devices have been used to excellent effect in numerous applications, including single-cell sequencing,[4,5] digital diagnostics,[6,7] nanoparticle synthesis,[8,9] drug screening,[10] directed evolution[11] and enzyme kinetic analysis.[12]

Droplets can be generated in either a passive or active manner. Passive methods, that leverage geometric variations in microchannel structures have proved to be exceptionally effective in allowing the robust generation of pL-volume droplets at high speeds. The most common passive methods, include the use of T-junctions,[13,14] flow focusing geometries,[15] and coflow structures.[16] Under certain circumstances, these geometries can be used to generate femtoliter (fL)-volume droplets via tip-streaming.[17] Although, fL-volume droplets can be formed in a robust manner, it is exceptionally difficult to control both droplet volumes and generation frequencies at the same time.[18] In this regard, step-emulsification strategies provide some advantage, since droplet size is primarily controlled by the geometry and size of the microchannel itself, with only a weak dependence on the flow conditions.[19] Although, step-emulsification has been shown to be effective in generating fL-volume droplets at high speed,[20] it should be noted that the strategy is poorly suited for controlling droplet payloads.

Active droplet generation methods are based on the principle of introducing additional energy into the fluidic system via mechanical, thermal, electrical, or optical means.[21–24] When compared to passive methods, active methods offer improved flexibility in regard to controlling droplet size and payloads, and in some cases enable on-demand droplet generation.[18] Amongst active strategies, pneumatic valving has been shown to be effective in generating,[25] splitting,[26] sorting,[27] and merging[25] droplets. Large numbers of pneumatic valves can be integrated within microfluidic devices, and typically comprise a control channel layer and flow channel layer, separated by a thin membrane.[28] The flow and control channels are aligned vertically, with the shared membrane between them acting as the valve. When pressure is applied to the control channel, the membrane is deformed and the flow is interrupted. Multiple valves can be integrated into a single device at high densities owing to the small size of each unit.[29] Microscale valves have proved to be exceptionally useful when performing complex experimental workflows. They can be used to isolate functional components and perform a range of droplet manipulations, including sorting, isolation, immobilization, and coalescence.[30] Through careful design, the operation of each individual functional unit can occur in isolation

T. Xue
College of Life Sciences
Northwest University
Xi'an, Shaanxi 710127, China
A. Jain, X. Cao, D. Hess, S. Stavrakis, A. deMello
Institute of Chemical and Bioengineering
ETH Zurich
Zurich 8093, Switzerland
E-mail: stavros.stavrakis@chem.ethz.ch; andrew.demello@chem.ethz.ch
X. Cao
Guangzhou Laboratory
Guangzhou, Guangdong 510320, China

and without influencing upstream or downstream operations.[31] Additionally, dead volumes are much lower than those associated with conventional pump-based droplet platforms. Since all tubing parts connected to the microfluidic inlets were prefilled, the dead volume in the current system is determined by the dimensions of the inlet channels and on the order of a few nLs. In simple terms, the use of pneumatic valves in droplet generation is based on establishing a difference between the valving pressure induced in the control channel and the overall pressure generated in the flow channel. Importantly, integrated microvalves have been shown to be effective in generating monodisperse droplet populations and have millisecond response times.[24] However, it should be noted that to date pneumatic valve-based droplet generators have been unable to generate fL-volume droplets in a controllable manner. With a view to realizing the on-demand production of fL-volume droplet populations, we herein describe the fabrication and testing of a novel active droplet generator, based on a V-valve construct.[32] We demonstrate the utility of the system in two applications central to multistep experimental workflows, namely, the titration of fluid samples with fL volume droplets and precise droplet dilution through sequential liquid exchanging. In both applications, the marriage of droplet-based and valve-based microfluidic principles provides a direct route to balancing controllability and analytical throughput.

2. Results and Discussion

2.1. Generation of Femtoliter Droplets

As shown in **Figure 1**a, the V-valve droplet generator comprises a V-valve[32] located above a semi-circular (Figure S1, Supporting Information) cross-section flow channel. The V-valve itself consists of two PDMS layers; a top fluidic layer and a bottom control layer. When pressure is applied to the control channel, the membrane between the two layers deforms. The characteristic V-shaped feature is able to completely seal the fluidic channel above a threshold pressure, but can also act as a "leaky" valve to trap or sieve particles when pressurized below this pressure.[32]

The threshold pressure is defined as the minimum pressure that will close the channel completely. This pressure will depend upon the geometry of the V-valve and the dimensions of the fluidic channel and can be determined experimentally. Importantly, the actuation pressure in the V-valve geometry can also generate significant shear on the immobilized droplet, which can lead to the formation of smaller "secondary" droplets with sub-pL volumes. To generate a series of fL-volume droplets, a nanoliter (nL) droplet is first immobilized in the V-valve geometry with the aid of an oil flow (Figure 1a). More specifically, a nL droplet is generated on-chip and then the V-valve pressure and the oil pressure values are used to immobilize the droplet at the V-valve geometry. To do this, a "low state" oil pressure is applied as soon as the generated droplet reaches the V-valve (Movie S1, Supporting Information). This oil flow pressurizes the nL droplet trapped in the V-valve. To subsequently generate fL droplets in an on-demand fashion, the oil pressure is modulated between "high" and "low" states. The "low state" corresponds to an oil pressure significantly below the threshold pressure, whilst the "high state" corresponds to a pressure significantly above the threshold pressure. A threshold oil pressure (typically between 65 and 85 mbar in the current system) is defined as the minimum oil pressure for a given V-valve pressure that allows the generation of secondary droplets. This is depicted in Figure 1b, where the size of the generated droplets is plotted as a function of the applied pressure from the oil phase and the V-valve pressure for a primary droplet of volume 150 pL.

As can be seen, the size of the generated droplet is strongly dependent on the actuation pressure of the V-valve between 800 and 1200 mbar, and weakly dependent on the oil pressure between 60 and 85 mbar. Droplet size and the V-valve pressure are inversely related, with a minimum average droplet diameter of 6 μm (110 fL volume) being achieved at a pressure of 1200 mbar. For oil pressures above 75 mbar, average droplet diameters decrease from 28 μm to 6 μm (11.5 pL to 110 fL) as the V-valve pressure varies between 800 and 1200 mbar. Alternatively, for a V-valve pressure of 800 mbar, average droplet diameters increase from 25 to 28 μm (8 to 11.5 pL) as the oil
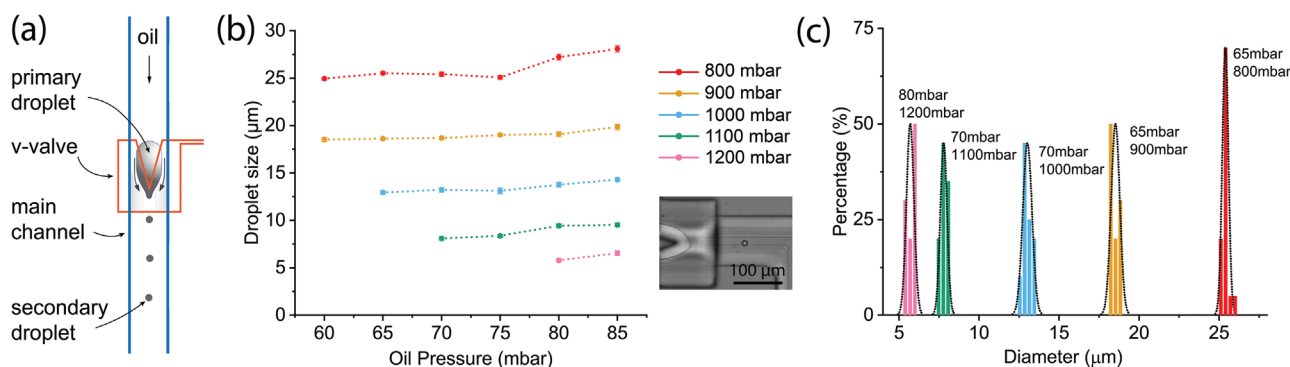

Figure 1. V-valve characterization. a) Schematic of the V-valve-based droplet generator. A primary (nL) droplet is first immobilized in the V-valve geometry and then pressurized by a stream of oil to generate secondary (fL to pL) droplets. b) Variation of the size of the generated droplets as a function of the applied pressure on the V-valve at various oil pressures and for a primary droplet of volume 150 pL. The size of generated droplets decreases with V-valve pressure and increases with the oil pressure. When the V-valve pressure is varied between 800 and 1200 mbar and the pressure on the oil is varied from 60 mbar to 85 mbar, the diameter of the generated droplets ranges from 28 to 6 μm (11.5 pL to 110 fL). (c) Droplet diameters are produced in the V-valve geometry for various combinations of V-valve and oil pressures. Histograms are fitted to normal distributions, with means at 5.7 ± 0.23 μm (1200, 80 mbar), 7.8 ± 0.19 μm (1100, 70 mbar), 13 ± 0.28 μm (1000, 70 mbar), 18.5 ± 0.27 μm (900, 65 mbar), 25.4 ± 0.19 μm (800, 65 mbar).

pressure varies between 65 and 85 mbar. We quantified the variations in droplet size, at *V*-valve pressures between 800 and 1200 mbar and oil pressures between 65 and 80 mbar. Droplet diameter distributions at different *V*-valve pressures and oil pressures are presented in Figure 1c and indicate robust droplet formation for a range of oil/*V*-valve pressures.

2.2. V-Valve Based Broplet Titrations

The controlled injection of reagents into a micron-sized droplet within a microfluidic device is a far from trivial task. Passive merging of droplets typically requires the synchronization of at least two generating flows to ensure reliable operation[35,36] and becomes cumbersome if multiple droplet types need to be merged in a specific sequence.[37,38] Additionally, it should be noted that pico-injection is an excellent method for the addition of reagents into preformed droplets,[39,40] it can become impractical if adjacent droplets need to be dosed with variable amounts of reagents. To address such limitations, we used the programmable droplet-based microfluidic system to perform on-demand droplet-based titrations (Figure S3, Supporting Information). The workflow is simple. Initially, fL to pL volume droplets are generated using a *V*-valve. These droplets are then merged with an immobilized droplet of user-defined volume. Such an approach allows the selective tuning of the content of the immobilized droplet by the injection of a controlled number of smaller droplets. Specifically, titration is achieved using a *V*-valve, an encapsulation chamber and electrode pair (**Figure 2**a). The encapsulation chamber has a higher height than the rest of the fluidic channel (Figure 2b) to ensure that

the droplet remains immobilized when inside the chamber. The salt electrodes are height matched with the encapsulation chamber, so as to assure effective electrofusion. The droplet titration process is summarized in Figure 2c-j and shown in Movie S2, Supporting Information. First, an 80 μm diameter water droplet is trapped in the encapsulation chamber. Next, fL to pL volume droplets (containing Alexa Fluor 488 at 50 μM) are sequentially generated at the *V*-valve with the side valve closed. The side valve in the open state provides an alternative flow path for the 80 μm water droplet to enter the encapsulation chamber and aids in its retrieval from the chamber. When a small (dye-filled) droplet reaches the trapped droplet, a square voltage pulse (1000 Hz, 600 V) is used to merge the droplets inside the encapsulation chamber. This process can be repeated multiple times to precisely control the payload of the trapped droplet, and is only limited by the maximum volume of the trapped droplet, which is defined by the size of the encapsulation chamber (380 pL). Afterward, the side valve is opened and a high pressure is applied on the oil phase to push the trapped droplet out for potential downstream analysis. The total duration of the titration process depends upon the droplet generation rate which can be as high as 19 Hz.

Figure 3 presents titration curves describing the addition of (variable volume) Alexa 488-containing droplets to a 0.27 nL trapped droplet. The average fluorescence emission is measured after each merging event and reflects the stepwise titration process. Specifically, droplets with diameters of 6.2, 8, 8.6, and 14.6 μm (and volumes of 125 fL, 268 fL, 333 fL, and 1.63 pL, respectively) were used for each titration. As can be seen, the addition of 128, 50, 33, 50, and 12 injected droplets (for the 6.2, 8, 8.6, and 14.6 μm diameter droplets, respectively) are needed
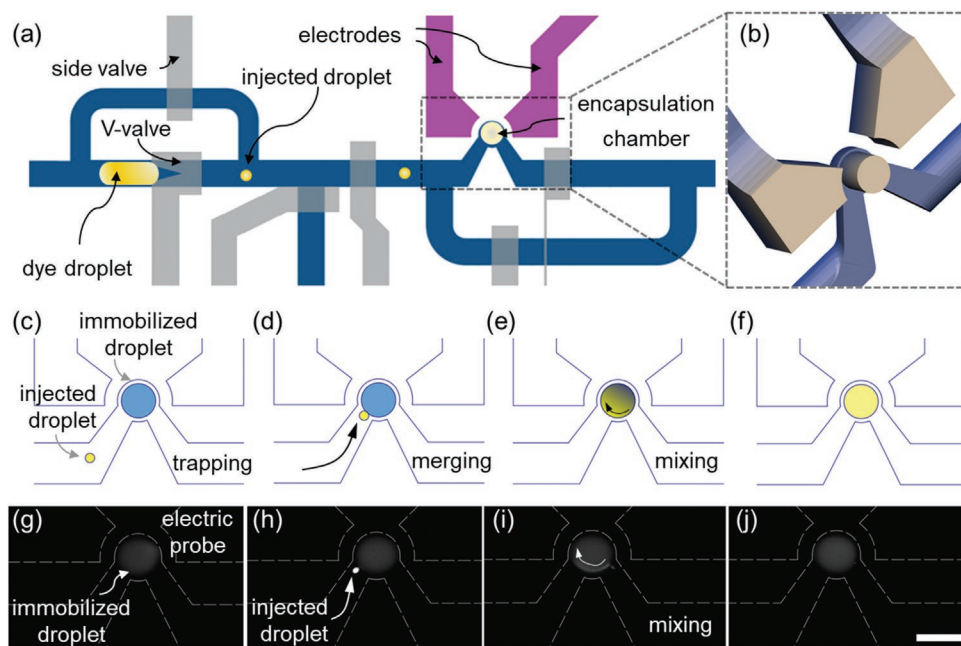

Figure 2. *V*-valve-based droplet titration. a) Schematic illustration of the titrator, consisting of a V valve geometry for the production of fL droplets and an encapsulation chamber where titration of the trapped nL-volume droplet occurs. b) Enlarged image of the encapsulation chamber and electrodes. c-j) Schematics and corresponding images of the titration process. A nL-volume droplet is located in the encapsulation chamber (c and g) and a fL-volume droplet approaches the immobilized droplet (d and h). Application of an electric field destabilizes the droplet interface allowing its coalescence with the fL-volume droplet and subsequent mixing (e, i). Titration is completed after mixing (f, j). Scale bar is 100 μm.
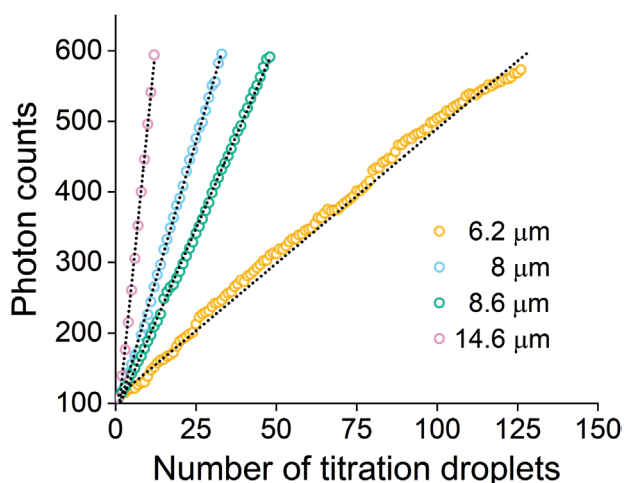
**ADVANCED
SCIENCE NEWS**
www.advancedsciencenews.com

**ADVANCED
MATERIALS
TECHNOLOGIES**
www.advmattechnol.de

Figure 3. Droplet titration curves. Variation of fluorescence intensity of the trapped nL droplet as a function of the number of titrating droplets containing Alexa 488 dye. Each curve shows a stepwise titration process, where fluorescence is measured after each merging event. When using droplets with diameters of 6.2, 8, 8.6, and 14.6 µm (and volumes of 125 fL, 268 fL, 333 fL, and 1.63 pL, respectively) 128, 50, 33, and 12 injected droplets are needed to generate a signal of 600 photon counts, respectively.

to generate an arbitrary signal of 600 photon counts. Moreover, in the case of the 6.2 µm diameter (125 fL) droplets, the volume ratio between the immobilized droplet (268 pL) and the input droplet is 2144. Other chip-based dilution approaches, such as the one reported by Niu and coworkers, use a volume ratio of ≈10.[41] This means that very small changes in droplet concentration can be realized in a rapid and precise manner.

2.3. Double V-Valve Droplet Dilution

Dilution is a basic and important process in most experimental workflows. Droplet-based microfluidic platforms have been shown to be useful tools for creating concentration gradients based on a droplet merging, mixing, and splitting paradigm. An elegant example of a droplet dilutor was reported by Niu and coworkers. Here, a large "mother" droplet is loaded with analyte at high concentration and localized in an asymmetric trapping chamber.[41] When an input (analyte-free) droplet is delivered to the trapping chamber, it merges with the mother droplet, ultimately generating a "daughter" droplet of a defined concentration. Such an approach was shown to be highly adept in creating user-defined concentration gradients of over four orders of magnitude and using only a small number of droplets. In a similar manner, Garstecki and colleagues reported a droplet dilutor that operates by passing a sample droplet through a series of diluent droplets located in trapping units.[42] Although efficient in function, both of these passive diluters cannot support the formation of concentration gradients when the volume ratio between the mother and input droplet is large. To address this limitation, we fabricated a droplet diluter based on a double V-valve construct (Figure S4, Supporting Information). Such a structure provides for high-precision droplet dilution through a sequential liquid exchange. As shown schematically in **Figure 4**a, a mother droplet of a defined concentra-

tion is localized within the microfluidic system. Small droplets containing only buffer are generated and then directed toward the trapped mother droplet. Through a process of droplet merging, mixing, and resplitting, the mother droplet can be used to generate a sequence of output or "daughter" droplets that define a digital concentration gradient. Since the volume of an incoming droplet is the same as the associated daughter droplet, the payload concentration in a daughter droplet after n dilution steps is given by:

$$C_n = \left(\frac{V_m}{V_m + V_c} \right)^n C_0 \tag{1}$$

$$n = 1 + \frac{\log \frac{C_n}{C_0}}{\log \left(\frac{V_m}{V_m + V_c} \right)} \tag{2}$$

where V_m and V_c are the volume of the mother and daughter droplets, respectively, C_0 and C_n are the concentrations of the mother droplet at the initial state and after n steps of dilution, respectively.

As shown in Figure 4b, the V-valve-based dilution system contains three inlets for reagent (in this case ink), the discrete phase (water), and the continuous phase (oil). These connect to the main channel via three independent control valves (Figure S4, Supporting Information). Two V-valves (V-valve 1 and V-valve 2) are located in the main channel with both integrating their own bypass side channel. The liquid electrodes filled are with 4 M NaCl solution and located on either side of V-valve 2. All of the channels are initially filled with oil prior to the experiment, except for the inlets containing water and ink. Application of 150 mbar to the ink and water channels and 120 mbar to the oil channel is used to generate two droplets (an ink droplet and a water droplet) that are trapped at the two V-valve structures. Specifically, the pressure on all the control valves is set to 1.2 bar. Application of a 30 ms pressure pulse to the ink valve (whilst keeping the oil valve open) allows the generation of a 580 pL ink droplet in the main channel. Side valve 2 is then closed and the ink droplet is driven toward V-valve 2. Using an identical procedure, a 620 pL water droplet is generated and trapped at V-valve 1 (Figure 4b). Next, application of 900 and 800 mbar to V-valve 1 and V-valve 2, respectively, is used to generate pL water droplets at V-valve 1 and merge these with the ink droplet at V-valve 2. More specifically, actuation of the oil valve for 50 ms (whilst keeping side valve 1 closed and side valve 2 open) is used to generate a 50 pL droplet (Figure 4c), which is then driven towards the large ink droplet (Figure 4d). Application of a sine-wave voltage (frequency 1 kHz, amplitude 600 V) to the positive electrode probe (for 500 ms) causes the merging of the smaller water droplet with the primary ink droplet (Figure 4e). Application of a 50 ms pulse to the oil valve, (whilst side valve 2 is closed and side valve 1 is open) generates a 50 pL droplet containing the diluted content from the ink droplet (Figure 4f). These droplets can be readily removed from the dilution module for downstream processing. Repetition of this process allows the production of a series of droplets of variable concentration. In this context, it should be noted that the
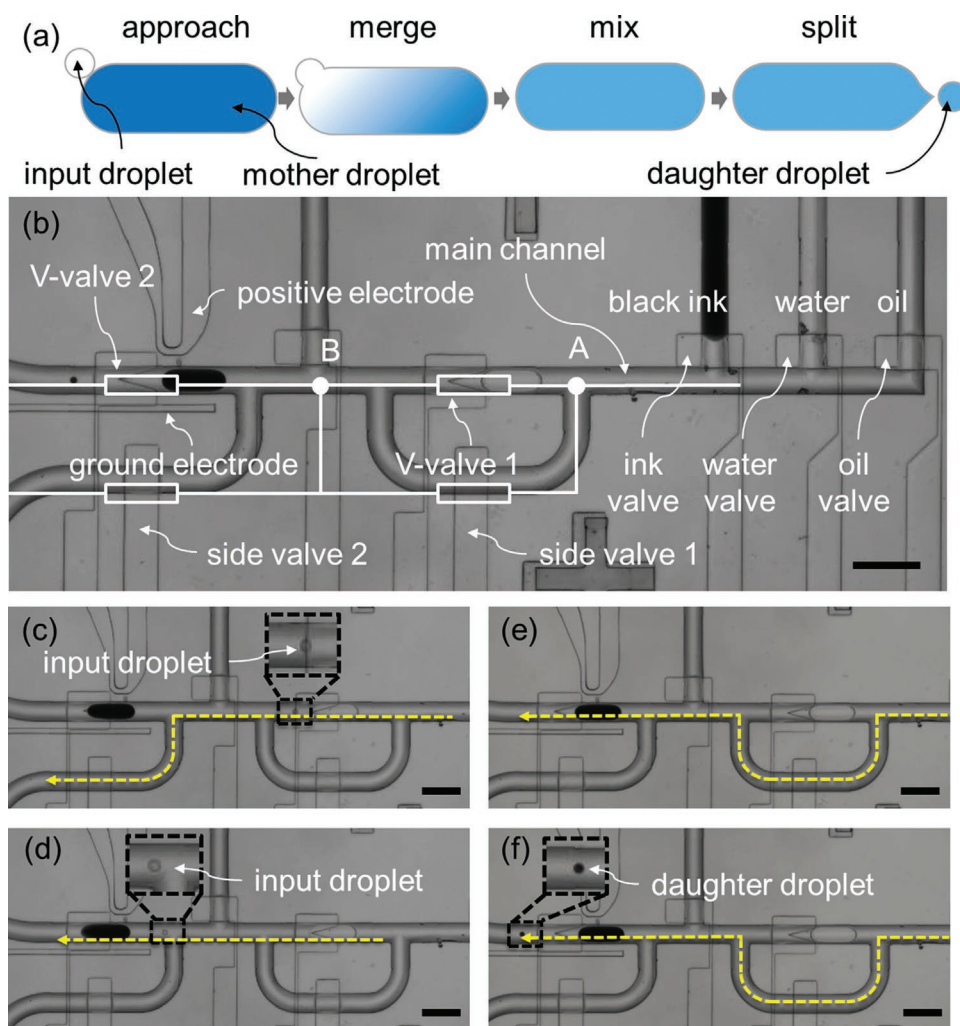
Figure 4. Operation of the double V-valve-based dilutor. a) Schematics of the droplet dilution process. An input fL droplet merges with the mother droplet and after mixing is completed a daughter droplet is produced with volume equal to the input droplet and concentration equal to the diluted mother droplet. b) Architecture of the double V-valve-based droplet dilutor, consisting of sample inlets, a main channel, V-valves, side channels, and electrodes. An ink droplet and water droplet are trapped by V-valve 1 and V-valve 2, respectively. c) An input droplet is generated at V-valve 1, whilst side valve 2 remains open. d) The input droplet approaches the droplet filled with ink with both bypass valves remaining closed. e) A high voltage is applied to the salt electrodes and the merging of the input droplet and the ink droplet occurs while side valve 1 is open. f) A daughter droplet splits from the ink droplet. All scale bars are 200 µm.

number of generated droplets, apart from the V-valve pressure, is also influenced by the volume of the mother droplet. Since it loses volume during operation, it is replaced every 20-dilution cycle. This is achieved by opening V-valve 1, the oil valve, and side valve 2 (Movie S3, Supporting Information).

Additionally, it should be noted that valve-containing side channels are placed alongside each V-valve to ensure the effective decoupling of each unit. Due to the serial-type connection of two V-valve units, adjusting the pressure parameters of both V-valves work during the dilution process can be quite challenging. To avoid such a situation, a side channel consisting of a valve is placed beside each V-valve geometry leading to the decoupling of two V-valve units as depicted in the channel routing (yellow dashed lines) of Figure 4c-f. For example, during droplet generation at V-valve 1, side valve 2 remains open to ensure that this operation does not influence the

immobilized droplet at V-valve 2 (Figure 4c). When both bypass valves are closed, the droplet produced by V-valve 1 slows down and approaches V-valve 2 (Figure 4d). In the case where side valve 1 is open, the pressure difference between points A and B is minimized (Figure 4e,f). In such a situation, the operation of V-valve 2 is independent of V-valve 1. To assess accessible dilution ratios, we performed fluorescence-based measurements by replacing ink with a 100 µM aqueous solution of Alexa 488 and fixed the mother droplet volume at 600 pL. Here a single round of dilution is a multistep process, consisting of the creation of a buffer droplet, merging the buffer droplet with the mother droplet, and splitting the (fluorescent) daughter droplet from the mother droplet. **Figure 5**a,b present dilution curves for 22.45 pL and 900 fL buffer droplets, respectively. As seen in Figure 5a, for the larger buffer droplets, 168 rounds of dilution are needed to dilute the mother droplet 33892-fold, as reported
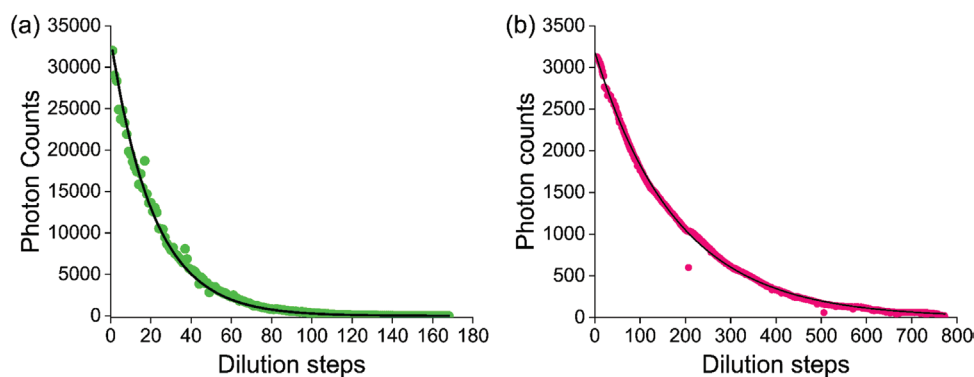
Figure 5. Dilution curves extracted from fluorescent daughter droplets were generated after splitting from the mother droplet. a) In the case of 35 µm diameter input droplets, the mother droplet is diluted 33892 times. b) In the case of 12 µm diameter input droplets, the concentration of the mother droplet is diluted by 859 times. Both fitting curves follow the dilution Equation (1) where the photon counts correspond to the initial concentrations of the mother droplet, C_0, and the dilutions steps are represented by n.

by fluorescence originating from the daughter droplets. For the 900 fL droplets, 773 rounds are required to dilute the sample concentration 859 times (Figure 5b). These data confirm the ability to generate bespoke concentration gradients using fL-volume input droplets. It should be noted that previous studies have shown that less than 23 daughter droplets can be used to dilute samples approximately 10^4 times.[41] Whilst undeniably useful in accessing wide concentration ranges, the double V-valve described herein provides a method for creating much higher resolution concentration gradients over narrower concentration ranges.

single-cell analysis.[43] For example, the current platform could be immediately used to maximize the information content associated with single-cell microfluidic experiments. Due to the ease with which V-valves can capture user-defined numbers of cells, investigations of cell-to-cell communications could be performed in a rapid and robust manner.[44] Moreover, the delivery of different reagents to such collections, would allow the direct monitoring of cellular responses to a range of environmental stimuli. To conclude, we believe that the programmable droplet modules described herein represent flexible and cost-effective tools for high-precision screening applications.

3. Conclusions

We have described the development of a new type of programmable microfluidic device possessing an unprecedented degree of fluid-handling precision. The on-demand droplet generator enables the production of fL-volume droplets with user-defined properties in a rapid and controllable fashion. The utility of V-valves in programmable droplet generation was showcased through programmable dilution and titration. Single droplets (with volumes as small as 125 fL) were generated and subsequently merged with a nL-volume sample droplet to generate a sequence of output droplets that define a digital concentration gradient. By tuning the pressure applied to both the V-valve construct and oil flow, the volume of the generated droplets can be adjusted to control the concentration gradient range and resolution. The approach provides unprecedented resolution in the dilution and titration of reagent mixtures. Importantly, the marriage of "traditional" and "programmable" droplet-based microfluidic concepts enables the a priori scheduling of droplets flows and on-demand droplet programming through valve actuation.

In conventional settings, titrations are performed using mL volumes of reagents. Here, using the same operational procedures, sample titrations and dilutions may be performed using reagent volumes over six orders of magnitude smaller and in a fraction of the time. Accordingly, we expect that the developed platform will have significant utility in a variety of biological and chemical workflows, such as digital PCR and

4. Experimental Section

Master Mold Fabrication: The master mold for the control channel layer, having a height of 15 µm, was fabricated in SU-8 (MicroChem, Ulm, Germany) on a standard silicon wafer and following standard lithographic procedures[33] (Figure S1, Supporting Information). Due to the multi-height nature and semi-circular cross-section of channels in the fluidic layer, two-photon polymerization 3D printing (Photonic Professional GT2, Nanoscribe, Eggenstein-Leopoldshafen, Germany) to fabricate the fluidic channel layer mold on ITO-coated glass was used.[34] Although features printed in this manner are of high resolution, they can occasionally detach from the glass substrate. To avoid such a situation, a 500 nm thick base layer of SU-8 2000 (MicroChem, Stuttgart, Germany) was used to improve the adhesion of the polymerized structure on the ITO-coated glass substrate. When printing, the laser scanning speed was set to 100 mm s^{-1}, with hatching and slicing distances of 0.5 µm and 1 µm, respectively. Polymerized structures were developed for 20 min using 1-Methoxy-2-propyl acetate (Sigma-Aldrich, Buchs, Switzerland). The fabricated master mold was then washed in isopropanol for 5 min, dried under a stream of nitrogen, and baked for 2 h at 150 °C.

PDMS Device Fabrication: Microfluidic devices were made from polydimethylsiloxane (PDMS) (Sylgard 184, Dow Corning, Dayton, USA). Prior to use, the control channel mold was treated with chlorotrimethylsilane (Sigma Aldrich, Buchs, Switzerland) in a vacuum chamber for 2 h, to inhibit adhesion to PDMS. A 20:1 mixture of PDMS monomer to curing agent (Sylgard 184, Dow Corning, Dayton, USA) was spin-coated at 2600 rpm onto the control channel mold for 40 s, allowed to stand at room temperature for 2 h and then baked at 70 °C for 30 min. Subsequently, a 5:1 mixture of PDMS monomer to curing agent was poured onto the fluidic channel mold, degassed, and cured for 20 min at 70 °C. After curing, the fluidic layer was peeled off the mold and diced into individual devices using a laboratory scalpel. Structured devices were then

**ADVANCED
SCIENCE NEWS**

www.advancedsciencenews.com

**ADVANCED
MATERIALS
TECHNOLOGIES**

www.advmattechnol.de

aligned and contacted with control layer structures under a stereoscope and then cured for 4 h at 70 °C to allow irreversible bonding of the two layers. Inlet and outlet ports were created at appropriate locations using a hole puncher (Technical Innovations, West Palm Beach, USA). The final PDMS device was plasma bonded to a glass slide after treating both surfaces in an EMITECH K1000X air plasma (Quorum Technologies, East Sussex, United Kingdom) for 60 s and kept in a 70 °C oven for 8 h.

Programmable Droplet Generation and Merging: The entire microfluidic platform system comprised a PC, an Uno R3 Arduino board (Distrelec, Nänikon, Switzerland), MH1 solenoid valves (Festo, Esslingen, Germany), a home-made board for controlling the solenoid valves, a TREK Model 2210 high-voltage amplifier (Acal BFi, Gröbenzell, Gemany), an OB1pressure pump (ELVESYS, Paris, France) and the microfluidic device itself (Figure S2, Supporting Information). The continuous phase for droplet formation consisted of HFE 7500 oil supplemented with 1% fluorosurfactant (RAN Biotechnologies, Boston, USA). On-chip valves were pressurized and depressurized using the solenoid valves, with an input pressure maintained at 1.2 Bar) and regulated by the Uno R3 Arduino board (Distrelec, Nänikon, Switzerland) and an in-house valve control board. The Arduino board was used to control the valves based on commands from in-house control software (written in C++). The board was also connected to the high-voltage amplifier, so as to allow voltage triggering during on-chip dielectrophoresis. To induce droplet merging, empty channels were converted to electrodes (positive and ground electrodes) by filling them with a 4 M NaCl salt solution.

Optical Measurements: Visualization experiments were performed using an inverted Ti–E fluorescence microscope (Nikon, Zurich, Switzerland). The acquisition of brightfield images was performed using a UI-3060CP-M-GL Rev.2 CMOS camera (IDS GmbH, Obersulm, Germany) operating at 30 frames per second (fps) in combination with a 10×, 0.3 NA Plan Fluor objective (Nikon, Zurich, Switzerland). Fluorescence images were acquired using an Andor Zyla sCMOS camera (Oxford Instruments, Oxford, UK) using the same 10x objective. A high-power SPECTRA X LED light source (Lumencor, Beaverton, USA) was used to excite the Alexa 488 dye, with emission being collected through Chroma 520/25 filter (AHF, Tübingen, Germany).

Supporting Information

Supporting Information is available from the Wiley Online Library or from the author.

Conflict of Interest

The authors declare no conflict of interest.

Author Contributions

T.X. and A.J. contributed equally to this work.

Data Availability Statement

The data that support the findings of this study are available from the corresponding author upon reasonable request.

[1] M. Srisa-Art, D.-K. Kang, J. Hong, H. Park, R. J. Leatherbarrow, J. B. Edel, S.-I. Chang, A. J. Demello, *ChemBioChem* **2009**, *10*, 1605.

[2] A. Suea-Ngam, P. D. Howes, M. Srisa-Art, A. J. Demello, *Chem. Commun.* **2019**, *55*, 9895.

[3] L. Bezinge, et al., *ACS Appl. Mater. Interfaces* **2018**, *10*, 18869.

[4] A. M. Klein, L. Mazutis, I. Akartuna, N. Tallapragada, A. Veres, V. Li, L. Peshkin, D. A. Weitz, M. W. Kirschner, *Cell* **2015**, *161*, 1187.

[5] H. N. Joensson, H. Andersson Svahn, *Angew. Chem.* **2012**, *51*, 12176.

[6] H. Yang, Z. Chen, X. Cao, Z. Li, S. Stavrakis, J. Choo, A. J. Demello, P. D. Howes, N. He, *Anal. Bioanal. Chem.* **2018**, *410*, 7019.

[7] H. Wu, X. Cao, Y. Meng, D. Richards, J. Wu, Z. Ye, A. J. Demello, *Biosens. Bioelectron.* **2022**, *211*, 114377.

[8] I. Lignos, S. Stavrakis, G. Nedelcu, L. Protesescu, A. J. Demello, M. V. Kovalenko, *Nano Lett.* **2016**, *16*, 1869.

[9] I. Lignos, R. M. Maceiczyk, M. V. Kovalenko, S. Stavrakis, *Chem. Mater.* **2020**, *32*, 27.

[10] A. Kulesa, J. Kehe, J. E. Hurtado, P. Tawde, P. C. Blainey, *Proc. Natl. Acad. Sci. USA* **2018**, *115*, 6685.

[11] A. Fallah-Araghi, J.-C. Baret, M. Ryckelynck, A. D. Griffiths, *Lab Chip* **2012**, *12*, 882.

[12] D. Hess, V. Dockalova, P. Kokkonen, D. Bednar, J. Damborsky, A. Demello, Z. Prokop, S. Stavrakis, *Chem* **2021**, *7*, 1066.

[13] P. Garstecki, M. J. Fuerstman, H. A. Stone, G. M. Whitesides, *Lab Chip* **2006**, *6*, 437.

[14] A. J. Demello, *Nature* **2006**, *442*, 394.

[15] M. Seo, C. Paquet, Z. Nie, S. Xu, E. Kumacheva, *Soft Matter* **2007**, *3*, 986.

[16] G. F. Christopher, S. L. Anna, *J. Phys. D: Appl. Phys.* **2007**, *40*, R319.

[17] J.-U. Shim, R. T. Ranasinghe, C. A. Smith, S. M. Ibrahim, F. Hollfelder, W. T. S. Huck, D. Klenerman, C. Abell, *ACS Nano* **2013**, *7*, 5955.

[18] P. Zhu, L. Wang, *Lab Chip* **2017**, *17*, 34.

[19] Z. Shi, X. Lai, C. Sun, X. Zhang, L. Zhang, Z. Pu, R. Wang, H. Yu, D. Li, *Chem. Commun.* **2020**, *56*, 9056.

[20] I. Kobayashi, S. Mukataka, M. Nakajima, *Ind. Eng. Chem. Res.* **2005**, *44*, 5852.

[21] Y. Zeng, M. Shin, T. Wang, *Lab Chip* **2013**, *13*, 267.

[22] K. Ahn, C. Kerbage, T. P. Hunt, R. M. Westervelt, D. R. Link, D. A. Weitz, *Appl. Phys. Lett.* **2006**, *88*, 024104.

[23] T. H. Ting, Y. F. Yap, N.-T. Nguyen, T. N. Wong, J. C. K. Chai, L. Yobas, *Appl. Phys. Lett.* **2006**, *89*, 234101.

[24] Z. Z. Chong, S. H. Tan, A. M. Gañán-Calvo, S. B. Tor, N. H. Loh, N.-T. Nguyen, *Lab Chip* **2016**, *16*, 35.

[25] S. Zeng, B. Li, X.'O. Su, J. Qin, B. Lin, *Lab Chip* **2009**, *9*, 1340.

[26] J.-H. Choi, S.-K. Lee, J.-M. Lim, S.-M. Yang, G.-R. Yi, *Lab Chip* **2010**, *10*, 456.

[27] Y. Chen, Y. Tian, Z. Xu, X. Wang, S. Yu, L. Dong, *Appl. Phys. Lett.* **2016**, *109*, 143510.

[28] S. J. Maerkl, S. R. Quake, *Science* **2007**, *315*, 233.

[29] R. Gómez-Sjöberg, A. A. Leyrat, D. M. Pirone, C. S. Chen, S. R. Quake, *Anal. Chem.* **2007**, *79*, 8557.

[30] K. Leung, H. Zahn, T. Leaver, K. M. Konwar, N. W. Hanson, A. P. Pagé, C.-C. Lo, P. S. Chain, S. J. Hallam, C. L. Hansen, *Proc. Natl. Acad. Sci. USA* **2012**, *109*, 7665.

[31] M. Vaninsberghe, H. Zahn, A. K. White, O. I. Petriv, C. L. Hansen, *PLoS One* **2018**, *13*, e0191601.

[32] H. S. Rho, Y. Yang, A. T. Hanke, M. Ottens, L. W. M. M. Terstappen, H. Gardeniers, *Lab Chip* **2016**, *16*, 305.

[33] D. Van Swaay, T.-Y. D. Tang, S. Mann, A. De Mello, *Angew. Chem., Int. Ed.* **2015**, *54*, 8398.

[34] X. Cao, et al., *Small* **n/a**(n/a): p. 1907534.

[35] J. Hong, M. Choi, J. B. Edel, A. J. Demello, *Lab Chip* **2010**, *10*, 2702.

[36] K. Churski, T. S. Kaminski, S. Jakiela, W. Kamysz, W. Baranska-Rybak, D. B. Weibel, P. Garstecki, *Lab Chip* **2012**, *12*, 1629.

[37] E. Brouzes, M. Medkova, N. Savenelli, D. Marran, M. Twardowski, J. B. Hutchison, J. M. Rothberg, D. R. Link, N. Perrimon, M. L. Samuels, *Proc. Natl. Acad. Sci. USA* **2009**, *106*, 14195.

[38] X. Niu, S. Gulati, J. B. Edel, A. J. Demello, *Lab Chip* **2008**, *8*, 1837.

[39] E. X. Ng, M. A. Miller, T. Jing, D. A. Lauffenburger, C.-H. Chen, *Lab Chip* **2015**, *15*, 1153.

[40] B. O'donovan, D. J. Eastburn, A. R. Abate, *Lab Chip* **2012**, *12*, 4029.

[41] X. Niu, F. Gielen, J. B. Edel, A. J. Demello, *Nat. Chem.* **2011**, *3*, 437.

[42] W. Postek, T. S. Kaminski, P. Garstecki, *Analyst* **2017**, *142*, 2901.

[43] C. M. Hindson, J. R. Chevillet, H. A. Briggs, E. N. Gallichotte, I. K. Ruf, B. J. Hindson, R. L. Vessella, M. Tewari, *Nat. Methods* **2013**, *10*, 1003.

[44] T. Chakraborty, S. M. Bartelt, J. Steinkühler, R. Dimova, S. V. Wegner, *Chem. Commun.* **2019**, *55*, 9448.